JOURNAL OF SOLID STATE CHEMISTRY **125,** 192–199 (1996)
ARTICLE NO. 0285

$K_{7-x-y}Ba_yNb_{14}P_9O_{60}$ ($x = 0.27(5)$, $y = 0.63(3)$), a Niobium Phosphate Bronze: Synthesis, Structure, and Physical Properties

J. Xu, T. Emge, K. V. Ramanujachary[1], P. Höhn, and M. Greenblatt[2]

Department of Chemistry, Rutgers, The State University of New Jersey, Piscataway, New Jersey 08855

Received November 20, 1995; in revised form April 29, 1996; accepted May 9, 1996

Large dark blue plate-like single crystals of $K_{7-x-y}Ba_yNb_{14}P_9O_{60}$ ($x = 0.27(5)$, $y = 0.63(3)$) have been synthesized by a solid state technique. A single crystal X-ray diffraction study shows that it crystallizes in the orthorhombic space group *Pmma*(#51) with the lattice parameters $a = 36.809(3)$, $b = 10.596(1)$, and $c = 6.459(1)$ Å and $z = 2$. A full matrix least-squares refinement based on 2451 reflections for $I > 2\sigma(I)$ yielded $R(F) = 0.047$ and $R_w(F^2) = 0.114$. The title compound is isostructural with the previously reported $K_7Nb_{14+x}P_{9-x}O_{60}$ ($x = 0.13$). Among the five unique K atoms in the crystal structure of $K_7Nb_{14.13}P_{8.87}O_{60}$, only K(5) appears to be predominantly substituted by barium. $K_{6.10}Ba_{0.63}Nb_{14}P_9O_{60}$ shows semiconducting behavior with an activation energy of 0.16(1) eV. Magnetic susceptibility measurements on a collection of randomly oriented single crystals indicated Curie behavior with an effective magnetic moment of $\mu_{eff} = 1.30\ \mu_B/Nb^{4+}$. A comparison of the structure as well as the electrical transport and magnetic properties of $K_{6.10}Ba_{0.63}Nb_{14}P_9O_{60}$ with that of $K_7Nb_{14.13}P_{8.87}O_{60}$ is presented.

INTRODUCTION

Molybdenum oxide bronzes with low-dimensional properties have been studied for many years, since they possess very interesting physical properties, including quasi-low-dimensional metallic behavior, charge-density-wave induced metal/insulator or metal/metal instabilities, and superconductivity (1, 2). Recently, similar electronic properties (3) have been observed in a number of phosphate tungsten bronzes (PTBs) with low-dimensional structures (4). More recently, several phosphate niobium bronzes (PNBs) with mixed valent niobium (IV/V) have been reported by Raveau and his co-workers (5). There are several structural similarities between PNBs and PTBs. The common structural units of these materials are corner-sharing MO_6 (M = Nb, W) octahedra to form infinite chains or ReO_3-type layers. The chains or ReO_3-like slabs are linked by PO_4 tetrahedra via corner sharing to give low-dimensional structures. Both PNBs and PTBs feature various kinds of tunnels that are created by the MO_6 and PO_4 polyhedral network, which can host alkali or alkaline earth cations. Because of the similarity of the structures of PNBs and PTBs, interesting low-dimensional properties were also expected in the PNB bronzes. However, in contrast to the PTBs which are metallic at room temperature, all the PNBs studied so far are semiconducting (6). For example, the $n = \infty$ member of the series $(K_3Nb_6P_4O_{26})_n \cdot KNb_2PO_8$, i.e., $K_3Nb_6P_4O_{26}$, shows anisotropic semiconducting behavior and Curie-like magnetic character (7). It appears that although the phosphate niobium bronzes have low-dimensional structures, the observed semiconducting behavior is due to the low Nb(IV) content, or charge carrier density. One way to increase the charge carrier concentration is to partially replace monovalent alkali cations with di- or trivalent cations. Since the effective size of K^+ ($r = 1.51$ Å, $CN = 8$) is comparable to that of Ba^{2+} ($r = 1.42$ Å, $CN = 8$) (8), substitution of Ba^{2+} for K^+ is expected to occur and increase the Nb(IV)/Nb(V) ratio and hence the density of carriers. In this paper we report the synthesis, crystal structure, and physical properties of the $n = 2$ member of the series $(K_3Nb_6P_4O_{26})_n \cdot KNb_2PO_8$, i.e., $K_7Nb_{14}P_9O_{60}$ (9), substituted by Ba^{2+}, $K_{6.10}Ba_{0.63}Nb_{14}P_9O_{60}$, and compare its crystal structure and physical properties with the parent compound $K_7Nb_{14.13}P_{8.87}O_{60}$ (9).

EXPERIMENTAL

Synthesis. Crystals of $K_{6.10}Ba_{0.63}Nb_{14}P_9O_{60}$ were grown in a reaction mixture intended to prepare the $m = 4$ member of the PNBs which is isostructural with monophosphate tungsten bronzes with pentagonal tunnels ($MPTB_p$) (10). A reaction mixture containing K_2CO_3 (Fisher, ACS certified grade), $BaCO_3$ (Johnson Matthey, 99.9%), Nb_2O_5 (Alfa, 99.5%), and $(NH_4)_2HPO_4$ (Fisher, 99.7%) in a molar ratio of 1.5 : 1 : 3.9 : 4 was ground in an agate mortar and heated at 400°C in a porcelain crucible overnight to remove CO_2, H_2O, and NH_3. The resulting powder was then mixed with

[1] Present address: Rowan College, Glassboro, New Jersey 08028-1701.
[2] To whom correspondence should be addressed.

0022-4596/96 $18.00

an adequate amount of niobium metal powder (Johnson Mattey Electronics, 99.8%) to achieve a composition of $K_3BaNb_8P_4O_{32}$, and was pelletized and sealed in an evacuated quartz tube. A charge of a 1.0 g pellet of the starting mixture in a 12 cm long (1.0 cm i.d. and 1.2 cm o.d.) evacuated quartz tube was placed into a muffle furnace horizontally, where a typical temperature gradient of about 50°C from end to end of the quartz tube was present, and was heated at 1200°C for 2 weeks, cooled at 5°C/hr down to 500°C, and then quenched to room temperature. Platelike, dark blue crystals with approximate dimensions of $0.90 \times 0.65 \times 0.35$ mm^3 grew at the cool end of the quartz tube. The crystals were washed in dilute HF (5 wt%) at 50°C before the physical property measurements. The composition of the crystals was determined by microprobe elemental analysis (JEOL, JXA-8600 Superprobe). No impurities (e.g., silicon) were detected.

A pellet of $K_{6.10}Ba_{0.63}Nb_{14}P_9O_{60}$ for the resistivity measurement was prepared in the following manner: several small crystals of $K_{6.10}Ba_{0.63}Nb_{14}P_9O_{60}$ were ground, pelletized, and sintered in an evacuated quartz tube at 950°C overnight. Polycrystalline $K_7Nb_{14.13}P_{8.87}O_{60}$ sample was prepared according to the method reported by Leclaire *et al.* (9). The pellet of $K_7Nb_{14.13}P_{8.87}O_{60}$ was sintered in an evacuated quartz tube at 1100°C for 2 days.

Powder X-ray diffraction (PXRD) patterns were recorded with a Scintag PAD V X-ray diffractometer using Cu$K\alpha$ radiation. Mica (NBS #675) powder was used as an internal standard. The PXRD pattern of $K_7Nb_{14.13}P_{8.87}O_{60}$ was indexed based on the space group *Pmma.* The cell parameters obtained for $K_7Nb_{14.13}P_{8.87}O_{60}$ by PXRD are $a = 36.813(5)$ Å, $b = 10.584(2)$ Å, and $c = 6.453(1)$ Å in good agreement with previous reports (9).

Single crystal X-ray diffraction. A plate shaped crystal of $K_{6.10}Ba_{0.63}Nb_{14}P_9O_{60}$ with dimensions $0.06 \times 0.10 \times 0.15$ mm^3 was selected for the structure determination. Data were collected with an Enraf Nonius CAD4 diffractometer at room temperature. Cell parameters and the orientation matrix for data collection were measured from 25 centered reflections in the range $9° < 2\theta < 31°$. No significant decay of the crystal was observed. The intensity data were corrected for Lorentz effects and polarization. An absorption correction was applied based on the bounding faces of the crystal, and the transmission factors were in the range from 0.584 to 0.808. There were 3813 unique data of which 2451 had $I > 2\sigma(I)$. The observed systematic absences $h = 2n + 1$ for the $hk0$ zone were consistent with the chosen space group *Pmma* (#51). The structure was refined using the SHELXL-93 (11) program. The final electron density map had a maximum peak of 1.7 e/Å^3 and a minimum of -2.0 e/Å^3 close to the K(5)/Ba(5) atom.

Crystal data and structure refinement results for $K_{6.10}Ba_{0.63}Nb_{14}P_9O_{60}$ are given in Table 1. Final positional parameters and the partial occupancy of K/Ba are listed in Tables 2 and 3; the selected bond distances are presented in Table 4.[3]

TABLE 1
Summary of Crystal Data and Structure Refinement Results for $K_{6.10}Ba_{0.63}Nb_{14}P_9O_{60}$

1. Crystal data	
Formula	$K_{6.10}Ba_{0.63}Nb_{14}P_9O_{60}$
Space group	*Pmma*
Cell dimensions (Å)	$a = 36.809(3)$
	$b = 10.596(1)$
	$c = 6.459(1)$
Volume (Å^3)	2519.2(6)
Z	2
2. Intensity measurements	
λ (Mo$K\alpha$) (Å)	0.71073
Scand mode	$\omega - \theta$
Total data collected	4455
Max 2θ (°)	60
Standard reflections	3 measured every 7200 s
Reflection with $I > 2\sigma(I)$	2451
μ (cm^{-1})	44.6
3. Solution and refinement	
Data/parameters	3813/232
Agreement factors $[I > 2\sigma(I)]^a$	$R_{(F)} = 0.051$ $R_{w(F^2)} = 0.118$
Agreement factors [all data][a]	$R_{(F)} = 0.099$ $R_{w(F^2)} = 0.127$
Goodness-of-fit on F^{2b}	1.04
Residual peaks (e/Å^3)	1.6, -2.3

[a] $R_{(F)} = \Sigma||F_o| - |F_c||/\Sigma|F_o|$, $R_{W(F^2)} = \{\Sigma[w(F_o^2 - F_c^2)^2]/\Sigma[w(F_o^2)^2]\}^{1/2}$.
[b] G. O. F. $= \{\Sigma(w(F_o^2 - F_c^2)^2)/(N_{obs} - N_{parm})\}^{1/2}$.

Physical property measurements. Electrical resistivity measurements on a single crystal of $K_{6.10}Ba_{0.63}Nb_{14}P_9O_{60}$ ($\sim 0.90 \times 0.65 \times 0.35$ mm^3), as well as on pellets of the polycrystalline $K_{6.10}Ba_{0.63}Nb_{14}P_9O_{60}$, and $K_7Nb_{14.13}P_{8.87}O_{60}$, were made by a standard four-probe technique with a Displex Cryostat (APD cryogenics, model DE 202) in the temperature range 60–300 K. Copper leads and silver print were used to make ohmic contacts to the samples. The I-V profiles were recorded at different temperatures to ensure the ohmic nature of the contacts.

Magnetic susceptibility data on a collection of randomly oriented single crystals of $K_{6.10}Ba_{0.63}Nb_{14}P_9O_{60}$ and polycrystalline of $K_7Nb_{14.13}P_{8.87}O_{60}$ were recorded with a Quan-

[3] Tables giving complete crystallographic details, bond lengths and angles, anisotropic thermal parameters, and calculated and observed structural factors are available as supplementary material. See NAPS document No. 05236 for 35 pages of supplementary materials. Order from ASIS/NAPS, Microfiche Publications, P.O. Box 3513, Grand Central Station, New York, NY 10163. Remit in advance $4.00 for microfiche copy or for photocopy, $7.75 up to 20 pages plus $.30 for each additional page. All orders must be prepaid. Institutions and Organizations may order by purchase order. However, there is a billing and handling charge for this service of $15. Foreign orders add $4.50 for postage and handling, for the first 20 pages, and $1.00 for additional 10 pages of material, $1.50 for postage of any microfiche orders.

TABLE 2
Atomic Fractional Coordinates and Equivalent Isotropic Displacement Coefficients (Å^2) for $K_{6.10}Ba_{0.63}Nb_{14}P_9O_{60}$[a]

Name	Wyckoff position	*x*	*y*	*z*	*U* (equiv)[b]
Nb1	8*l*	0.44504(2)	0.17625(6)	0.24195(9)	0.0089(1)
Nb2	8*l*	0.34237(2)	0.17737(6)	0.2534(1)	0.0120(2)
Nb3	4*j*	0.44652(3)	0.5000	0.0178(1)	0.0144(2)
Nb4	4*k*	0.2500	0.18310(9)	0.4544(2)	0.0152(2)
Nb5	4*j*	0.34197(3)	0.5000	0.0421(2)	0.0133(2)
P1	8*l*	0.67565(5)	0.2378(2)	0.2466(3)	0.0111(3)
P2	8*l*	0.53928(4)	0.2372(2)	0.2548(3)	0.0068(3)
P3	2*f*	0.2500	0.5000	0.2723(7)	0.0166(8)
K1	4*i*	0.60721(6)	0.0000	0.2580(4)	0.0284(8)
Ba1	4*i*	0.60721(6)	0.0000	0.2580(4)	0.0284(8)
K2	2*e*	0.2500	0.0000	−0.0439(7)	0.048(2)
Ba2	2*e*	0.2500	0.0000	−0.0439(7)	0.048(2)
K3	2*d*	0.5000	0.5000	0.5000	0.025(2)
K4	4*j*	0.39012(8)	0.5000	−0.4715(4)	0.042(1)
Ba4	4*j*	0.39012(8)	0.5000	−0.4715(4)	0.042(1)
K5	2*f*	0.2500	0.5000	−0.2265(3)	0.0304(7)
Ba5	2*f*	0.2500	0.5000	−0.2265(7)	0.0304(7)
O1	8*l*	0.3957(1)	0.1610(5)	0.2355(8)	0.016(1)
O2	8*l*	0.4416(1)	0.3670(4)	0.2030(7)	0.011(1)
O3	8*l*	0.5530(1)	0.1608(4)	0.0686(7)	0.014(1)
O4	8*l*	0.4986(1)	0.2255(4)	0.2688(8)	0.015(1)
O5	8*l*	0.5578(1)	0.1816(4)	0.4479(7)	0.0119(9)
O6	4*i*	0.4560(2)	0.0000	0.251(1)	0.012(1)
O7	4*i*	0.3404(2)	0.0000	0.290(1)	0.022(2)
O8	8*l*	0.6611(1)	0.1612(4)	0.0582(8)	0.016(1)
O9	8*l*	0.6517(1)	0.2024(5)	0.4374(7)	0.014(1)
O10	8*l*	0.3466(1)	0.3630(4)	0.2226(7)	0.014(1)
O11	8*l*	0.2894(1)	0.1824(5)	0.2740(7)	0.015(1)
O12	8*l*	0.5516(1)	0.3748(4)	0.2388(7)	0.0116(9)
O13	2*b*	0.5000	0.5000	0.0000	0.013(2)[c]
O14	4*j*	0.3908(2)	0.5000	−0.040(1)	0.014(1)
O15	4*j*	0.2836(2)	0.5000	0.128(1)	0.020(2)
O16	8*l*	0.6731(2)	0.3783(5)	0.1980(9)	0.020(1)
O17	8*l*	0.7149(1)	0.2025(6)	0.2915(8)	0.020(1)
O18	4*k*	0.2500	0.3834(6)	0.421(1)	0.015(1)
O19	2*e*	0.2500	0.0000	0.491(2)	0.014(2)

[a] Estimated standard deviations of refined parameters are enclosed in parentheses.
[b] Atoms are refined anisotropically: $U_{(equiv)} = 1/3(U_{11}\, a^{*2}\, a^2 + U_{22}\, b^{*2}\, b^2 + U_{33}\, c^{*2}\, c^2 + U_{12}\, a^*\, b^*\, a\, b \cos\gamma + U_{13}\, a^*\, c^*\, a\, c \cos\beta + U_{23}\, b^*\, c^*\, b\, c \cos\alpha)$.
[c] Refined isotropically.

tum Design SQUID magnetometer in the temperature range 2–300 K. The applied magnetic field was 0.5 T. The susceptibility data were corrected for the core diamagnetic contributions of the component ions.

RESULTS AND DISCUSSION

Crystal structure. The pulverized crystals of $K_{6.10}Ba_{0.63}Nb_{14}P_9O_{60}$ were identified by PXRD to be isostructural with $K_7Nb_{14.13}P_{8.87}O_{60}$. The initial structural model was based on $K_7Nb_{14.13}P_{8.87}O_{60}$. The structural refinement shows that while the K(1), K(2), and K(4) sites have low partial occupancies of Ba (5.0, 3.2, and 7.6%, respectively), the K(5) position had a significant partial occupancy of Ba by 34.4%; the K(3) site is occupied solely by potassium with 26.4% vacancy. All other sites were fully occupied; no other partial or joint occupancies were detected. These values correspond to 6.10 for K and 0.63 for Ba per formula unit, i.e., $K_{6.10}Ba_{0.63}Nb_{14}P_9O_{60}$; this composition was in good agreement with that obtained by microprobe elemental analysis (JEOL, JXA-8600 Superprobe). The reliability of the refinement of the occupancy factors is supported by

TABLE 3
Result of Partial Occupancy Refinements[a]

Name	Occupancy
K(1)	0.475(2)
Ba(1)	0.025(2)
K(2)	0.242(2)
Ba(2)	0.008(2)
K(3)	0.184(4)
K(4)	0.462(3)
Ba(4)	0.038(3)
K(5)	0.164(2)
Ba(5)	0.086(2)

[a] Estimated standard deviations of refined parameters are enclosed in parentheses.

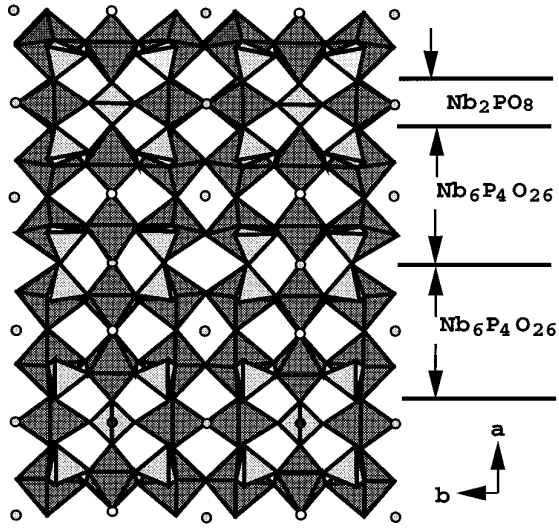

FIG. 1. Projection of $K_{6.10}Ba_{0.63}Nb_{14}P_9O_{60}$ in the *ab* plane. Blank circles represent K, shaded circles represent K/low Ba occupancy, and dark circles K/high Ba occupancy.

calculations of bond valence sums for the five K positions after Breese and O'Keeffe (12). Values between 0.83 and 1.05 v.u. for positions K(1) to K(4), but of 1.53 v.u. for the K(5) position are obtained, if all K–O bonds with bond valence sums >0.01 v.u. (12) are considered.

The crystal structure of the barium-substituted phosphate niobium bronze is similar to that of the parent compound $K_7Nb_{14.13}P_{8.87}O_{60}$ (9), in which $[Nb_2PO_8]$ units form infinite chains along the *b* axis and connect two successive $[Nb_6P_4O_{26}]$ slabs along the *a* axis to give a three-dimensional framework formulated as $[Nb_6P_4O_{26}]_2 \cdot Nb_2PO_8$ (Fig. 1). The cell parameters of these two phases are comparable, i.e., $a = 36.883(3)$, $b = 10.603(1)$, and $c = 6.4526(5)$ Å for $K_7Nb_{14.13}P_{8.87}O_{60}$ and $a = 36.809(3)$, b = 10.596(1), and $c = 6.459(1)$ Å for $K_{6.10}Ba_{0.63}Nb_{14}P_9O_{60}$.

TABLE 4
Bond Distances (Å) of NbO_6 and PO_4 in $K_{6.10}Ba_{0.63}Nb_{14}P_9O_{60}$[a]

Nb(1)–O(1)	1.827(5)	Nb(2)–O(1)	1.975(5)
–O(2)	2.042(5)	–O(7)	1.897(1)
–O(3)	2.016(4)	–O(8)	2.026(5)
–O(4)	2.049(5)	–O(9)	2.029(5)
–O(5)	2.009(4)	–O(10)	1.984(5)
–O(6)	1.913(2)	–O(11)	1.957(5)
Nb(3)–O(2) ×2	1.859(5)	Nb(4)–O(11) ×2	1.863(5)
–O(13)	1.975(1)	–O(19)	1.956(2)
–O(14)	2.087(7)	–O(17) ×2	2.101(5)
–O(12) ×2	2.126(5)	–O(18)	2.135(7)
Nb(5)–O(10) ×2	1.871(5)	P(1)–O(17)	1.522(5)
–O(16) ×2	2.094(5)	–O(16)	1.526(5)
–O(15)	2.222(8)	–O(8)	1.559(5)
–O(14)	1.875(7)	–O(9)	1.563(5)
P(2)–O(4)	1.508(5)	P(3)–O(15) ×2	1.549(8)
–O(12)	1.532(5)	–O(18) ×2	1.568(7)
–O(5)	1.540(5)		
–O(3)	1.536(5)		

[a] Estimated standard deviations are enclosed in parentheses.

In $K_7Nb_{14.13}P_{8.87}O_{60}$, five unique potassium atoms are located in the intersections of hexagonal tungsten bronze, brownmillerite, and perovskite-type tunnels formed by corner-sharing NbO_6 and PO_4 polyhedra. The comparable size of K and Ba allows Ba substitution for K at all the potassium sites of $K_7Nb_{14.13}P_{8.87}O_{60}$. However, no Ba was found at the K(3) sites in $K_{6.10}Ba_{0.63}Nb_{14}P_9O_{60}$. The reason for the preferential occupancy of Ba at the various K sites is not clear at present. It is likely that factors such as Coulomb interaction and lattice strain may play an important role.

It was reported that in $K_7Nb_{14.13}P_{8.87}O_{60}$ the P(3) tetrahedral site was randomly occupied by both P and Nb atoms resulting in the simultaneous existence of PO_4 and NbO_4 tetrahedra (9). In the Ba substituted analog studied in this work, the P(3) site appears to be occupied exclusively by P atoms. There are two P(3)–O bond distances of 1.549(8) Å and two of 1.568(7)Å, which are normal for P–O bonds in PO_4 tetrahedra in transition metal phosphates. Typical tetrahedral Nb–O bond distances are ~1.6 Å (13); the P(3)/(Nb)–O distances in the $K_7Nb_{14.13}P_{8.87}O_{60}$ compound are all 1.60(1) Å (9). It should be pointed out that in the sample of $K_7Nb_{14.13}P_{8.87}O_{60}$ by Leclaire *et al.* (9) silicon substitution for phosphorous may have taken place; i.e., these samples were heated at 1100°C for 1 month in evacuated quartz ampoules, so the incorporation of silicon into the bronze might be expected. If a reaction with the quartz

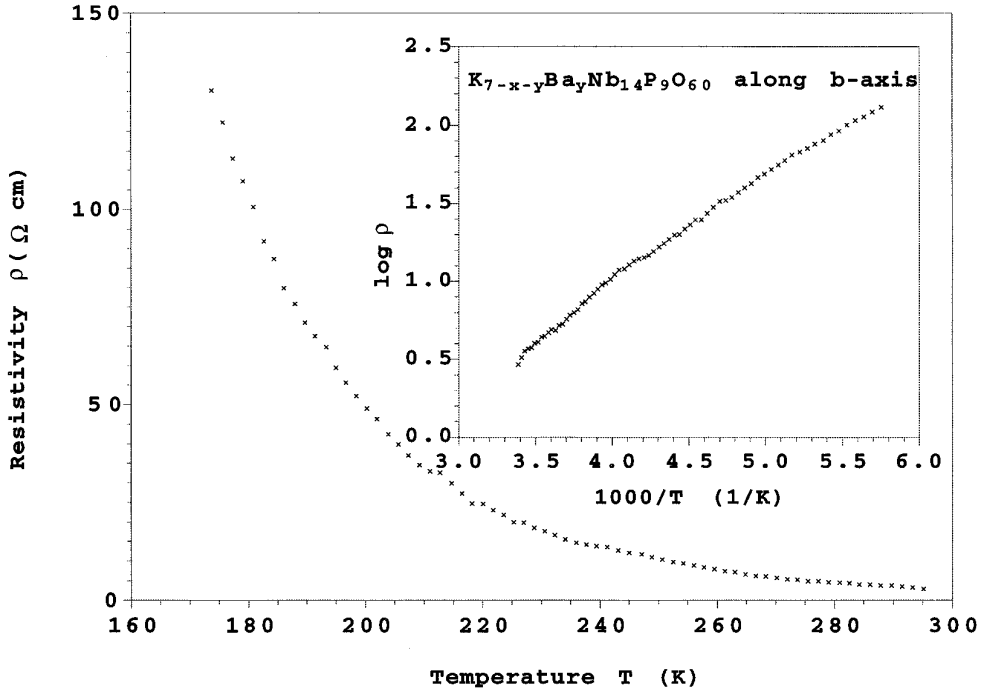

FIG. 2. The temperature dependent electrical resistivity along the *b* axis of a single crystal of $K_{6.10}Ba_{0.63}Nb_{14}P_9O_{60}$.

ampoule did occur, it could explain the large average P(3)–O distance observed (d(Si–O) = 1.60 Å) as well as the assumed substitution of P^{5+} by Nb^{5+} (9). We did not detect any silicon in the Ba substituted analog by chemical analysis, nor did the structure refinement suggest mixed occupancy on the P(3) site. However, a calculation of the bond valence sums after Brese and O'Keeffe (12) gives values of 4.75, 4.93, and 4.54 v.u. for P(1), P(2), and P(3), respectively, in the Ba substituted phase, whereas the values of Nb(1) to Nb(5) vary between 4.91 and 5.19 v.u. This result suggests that at least the P(3) position may be partially occupied by silicon.

Electrical resistivity. Figure 2 shows the electrical resistivity of a $K_{6.10}Ba_{0.63}Nb_{14}P_9O_{60}$ single crystal measured along the crystallographic *b* axis in the temperature range 160–300 K. The room temperature resistivity is 1.9(4) $\Omega \cdot$ cm, and increases exponentially with decreasing temperature indicating semiconducting behavior. The activation energy (E_a) estimated from the linear portion (300–200 K) of the plot of $\log \rho$ vs $1000/T$ is 0.15(1) eV. The resistivity perpendicular to the *bc* plane could not be measured with a four-terminal technique due to the smaller dimension of the crystals. However, a qualitative room temperature resistivity, using a two-probe technique, gave ρ_{RT} = 7.4(2) $\Omega \cdot$ cm. The observed anisotropy in the electrical conductivity is consistent with the anisotropy of the crystal structure. Along the *b* axis, corner-sharing NbO_6 octahedra form $[NbO_3]_\infty$ chains that favor the formation of a narrow conduction band and a possible delocalization of the charge carriers. This is consistent with the relatively smaller resistivity in this direction. In contrast, the infinite $[PNb_4O_{14}]$ chains containing strings of four corner-sharing octahedra separated by insulating PO_4 tetrahedra account for the higher resistivity observed along the *a* axis.

In order to compare the electrical resistivities of $K_{6.10}Ba_{0.63}Nb_{14}P_9O_{60}$ to those of $K_7Nb_{14.13}P_{8.87}O_{60}$, we have measured the temperature dependent resistivity of the pressed pellets of these two compositions (Fig. 3). It is evident that both compounds exhibit semiconducting behavior. The room temperature resistivities (Fig. 3) and the activation energies (E_a) (Table 5) show that $K_{6.10}Ba_{0.63}Nb_{14}P_9O_{60}$ has a higher resistivity and activation energy than $K_7Nb_{14.13}P_{8.87}O_{60}$. This is somewhat surprising in view of the increased Nb(IV)/Nb(V) ratio in $K_{6.10}Ba_{0.63}Nb_{14}P_9O_{60}$. In order to account for this anomalous behavior, we consider two major factors that affect the electrical resistivity: charge carrier density and mobility. The charge carrier density increases slightly from 0.14 e^-/Nb for $K_7Nb_{14.13}P_{8.87}O_{60}$ to 0.17 e^-/Nb for $K_{6.10}Ba_{0.63}Nb_{14}P_9O_{60}$, which should result in an increase of the conductivity of the latter. However, the contrastingly higher resistivity of $K_{6.10}Ba_{0.63}Nb_{14}P_9O_{60}$ indicates that the Ba sites may act as potential traps for the conduction electrons. Thus, in the substituted phase, the small increase in the charge carrier concentration is apparently more than offset by the Coulombic barriers resulting in higher resistivity.

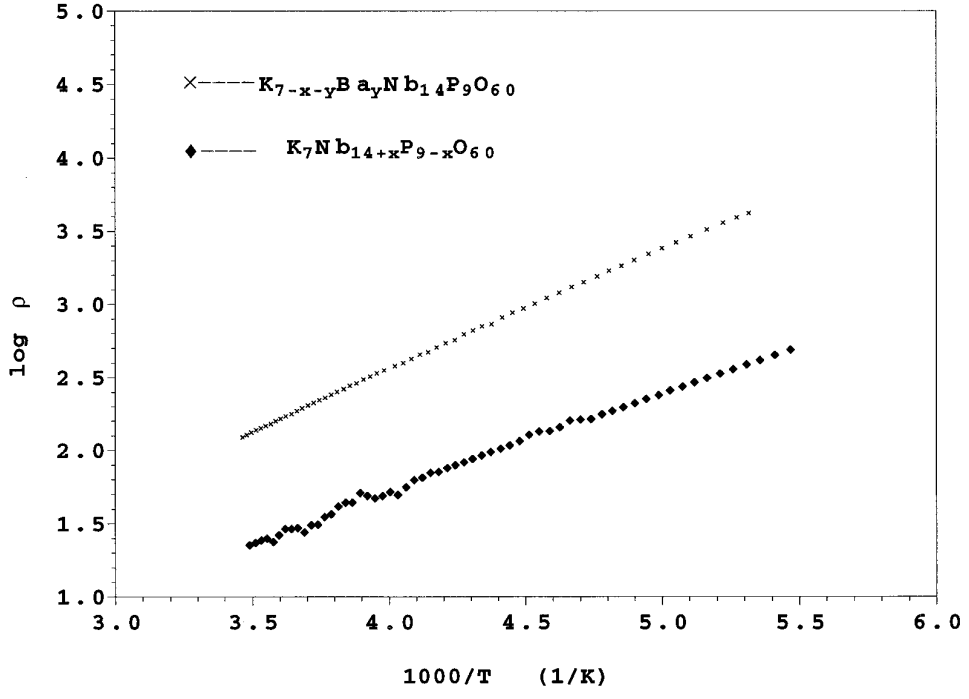

FIG. 3. Plots of log ρ vs $1000/T$ for the polycrystalline samples of $K_7Nb_{14.13}P_{8.87}O_{60}$ and $K_{6.10}Ba_{0.63}Nb_{14}P_9O_{60}$.

Magnetic susceptibility. The temperature dependent molar magnetic susceptibility of a batch of randomly oriented crystals of $K_{6.10}Ba_{0.63}Nb_{14}P_9O_{60}$ is shown in Fig. 4. The inset shows the variation of $1/\chi$ as a function of T. The susceptibility data were fitted to $\chi = C/T$, with a Curie constant $C = 0.500$ emu · K/mol and $\mu_{\text{eff}} = 1.30\ \mu_B/Nb^{4+}$ (assuming spin-only contribution). This effective magnetic moment is smaller than the theoretical value of 1.73 μ_B, which implies that only a fraction of the charge carriers are localized, while the remaining must be delocalized.

The variation of molar magnetic susceptibility of $K_7Nb_{14.13}P_{8.87}O_{60}$ in Fig. 5 in the inset details the portion of χ vs T which shows an anomaly around 100 K. In order to examine whether this anomaly is due to spin-glass-like behavior, we have carried out detailed magnetization measurements under zero field and field cooled conditions. The susceptibility remained independent of applied magnetic field, which suggests that the origin of this anomaly is not likely from a spin-glass-like behavior. The magnetic susceptibility in the $140 < T < 300$ K and $2 < T < 30$ K temperature regions could be fitted separately to a modified Curie–Weiss relationship according to

$$\chi = \chi_0 + C/(T - \theta).$$

where χ_0 are the temperature independent contributions such as Van Vleck, Pauli magnetism, and core diamagnetism, C is the Curie constant, and θ is the Curie–Weiss temperature. χ_0, C, and θ obtained by a nonlinear least-squares fitting of the observed data and the calculated effective magnetic moments are presented in Table 6. A small anomaly seen around 50 K in Fig. 5 arises from the antiferromagnetic ordering of absorbed O_2 (14). Above 140 K, the effective magnetic moment of 1.61 μ_B/Nb^{4+} (somewhat smaller than the spin-only value of 1.73 μ_B) is consistent with the presence of local moments associated with $4d^1$ electrons on Nb^{4+} sites in the structure. A magnetic correlation between these $4d^1$ electrons may be responsible for the antiferromagnetic ordering (AF) observed around 100 K. Furthermore, the effective magnetic moment below 30 K is 0.98 μ_B/Nb^{4+}, which is considerably smaller than that observed above 140 K (1.61 μ_B/Nb^{4+}). The smaller effective magnetic moment implies that a significant fraction of the electrons remain ordered below 100 K.

The contrast between the simple Curie magnetic behavior of $K_{6.10}Ba_{0.63}Nb_{14}P_9O_{60}$ and the antiferromagnetic or-

TABLE 5
Summary of the Electrical Transport Properties of Polycrystalline $K_{6.10}Ba_{0.63}Nb_{14}P_9O_{60}$ and $K_7Nb_{14.13}P_{8.87}O_{60}$

Composition	ρ_{RT} (Ω cm)	E_a (eV)
$K_{6.10}Ba_{0.63}Nb_{14}P_9O_{60}$	$1.2(2) \times 10^2$	0.16(1)
$K_7Nb_{14.13}P_{8.87}O_{60}$	$1.8(3) \times 10^1$	0.14(1)

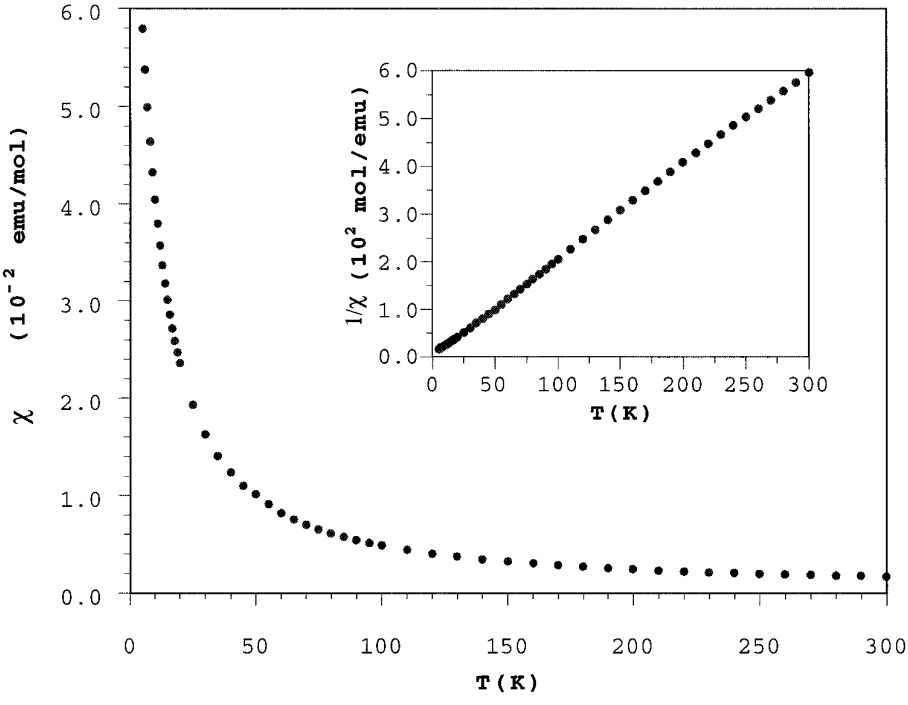

FIG. 4. The temperature dependent magnetic susceptibility of a collection of randomly oriented single crystals of $K_{6.10}Ba_{0.63}Nb_{14}P_9O_{60}$. Inset shows the plot of $1/\chi$ vs T.

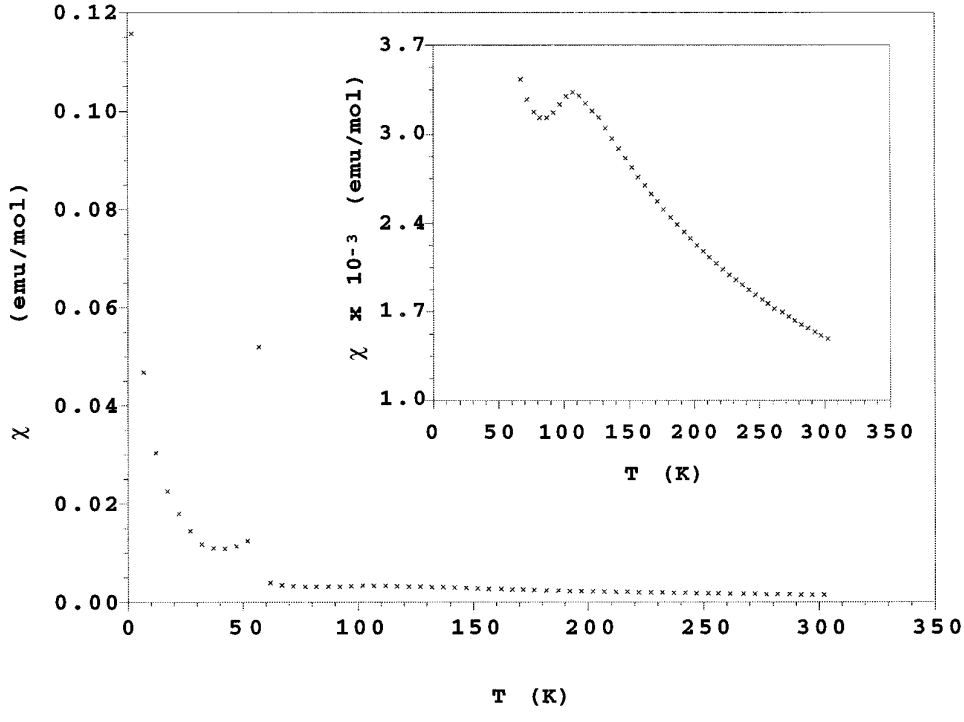

FIG. 5. The temperature dependent magnetic susceptibility of polycrystalline $K_7Nb_{14.13}P_{8.87}O_{60}$. Inset shows the susceptibility anomaly ~100 K.

TABLE 6
Summary of the Magnetic Susceptibility of Randomly Oriented Crystals of $K_{6.10}Ba_{0.63}Nb_{14}P_9O_{60}$ and Polycrystalline $K_7Nb_{14.13}P_{8.87}O_{60}$

Compounds	χ_0 (emu/mol)	θ (K)	C (emu · K/mol)	μ_{eff}/Nb^{4+} (μ_B)
$K_7Nb_{14.13}P_{8.87}O_{60}$ $T > 140$ K	−0.014	−60.15	0.647	1.61
$K_7Nb_{14.13}P_{8.87}O_{60}$ $T < 30$ K	−0.0086	−0.80	0.241	0.98
$K_{6.10}Ba_{0.63}Nb_{14}P_9O_{60}$	0	−2.03	0.500	1.30

dering at ~100 K in the unsubstituted phase may be attributed to the change in the local symmetry around the K/Ba sites and the number of the electrons per formula unit upon introducing barium into the lattice. The former (i.e., change of symmetry) may destroy the good overlap of d(Nb)–p(O) orbitals necessary for long range magnetic correlations, and the latter (i.e., Ba substitution) alters the band filling. The absence of AF ordering in the substituted sample may be attributed to both effects. Furthermore, the larger resistivity of the substituted sample is consistent with these arguments.

CONCLUSIONS

We have synthesized and characterized a phosphate niobium bronze, $K_{6.10}Ba_{0.63}Nb_{14}P_9O_{60}$, which is isostructural with $K_7Nb_{14.13}P_{8.87}O_{60}$. Barium ions partially substituted for potassium at the K(1), K(2), K(4), and K(5) sites. As a result of the barium substitution, the NbO_4 tetrahedra present in the unsubstituted phase are absent in the $K_{6.10}Ba_{0.63}Nb_{14}P_9O_{60}$. Both $K_7Nb_{14.13}P_{8.87}O_{60}$ and $K_{6.10}Ba_{0.63}Nb_{14}P_9O_{60}$ are semiconducting. The magnetic susceptibility studies of $K_7Nb_{14.13}P_{8.87}O_{60}$ show Curie–Weiss behavior and an anomaly around 100 K, which is attributed to weak antiferromagnetic ordering. $K_{6.10}Ba_{0.63}Nb_{14}P_9O_{60}$ exhibits simple Curie behavior.

ACKNOWLEDGMENTS

The authors thank one of the reviewers for pointing out by bond valence sum calculations that silicon may have substituted in the P(3) site both in $K_7Nb_{14.13}P_{8.87}O_{60}$ and $K_{6.10}Ba_{0.63}Nb_{14}P_9O_{60}$. Similarly, his calculations of bond valence sums for the five K positions are in good agreement with our partial occupancy refinement of the K positions. We have included his comments in our discussions.

This work was supported by the National Science Foundation—Solid State Chemistry Grant DMR-93-14605.

REFERENCES

1. M. Greenblatt, *Chem. Rev.* **88,** 31, (1988).
2. C. Schlenker, "Low-Dimensional Electronic Properties of Molybdenum Bronze and Oxides." Kluwer, Dordrecht, The Netherlands, 1989.
3. M. Greenblatt, *Int. J. Modern Phys. B* **7,** 3937, (1993).
4. B. Raveau, *Proc. Indian Nat. Sci. Acad. A* **52**(1), 67 (1986).
5. B. Raveau, M. M. Borel, A. Leclaire, and A. Grandin, *Int. J. Modern Phys. B* **7,** 4109, (1993).
6. A. Benabbas, J. Provost, M. M. Borel, A. Leclaire, and B. Raveau, *Chem. Matter.* **5,** 1143 (1993).
7. J. Xu, K. V. Ramanujachary, and M. Greenblatt, *Mater. Res. Bull.* **28,** 1153 (1993).
8. R. D. Shannon, *Acta Crystallogr. A* **32,** 751 (1976).
9. A. Leclaire, A. Benabbas, M. M. Borel, A. Grandin, and B. Raveau, *J. Solid State Chem.* **83,** 245 (1989).
10. G. Costentin, M. M. Borel, A. Grandin, A. Leclaire, and B. Raveau, *Mater. Res. Bull.* **26,** 1051 (1991).
11. G. M. Sheldrick, "SHELXL-93, Program for Crystal Structure Refinement." Univ. of Göttingen, Germany, 1993.
12. E. Brese and O'Keeffe, *Acta Crystallogr. B* **47,** 192 (1991).
13. B. M. Gatehouse and A. D. Wadsley, *Acta Crystallogr.* **17,** 1545 (1964).
14. Quantum Design Technical Advisory MPMS No. 8, Quantum Design, Inc. (1990).